CrystEngComm

Accepted Manuscript

ROYAL SOCIETY OF CHEMISTRY

www.rsc.org/crystengcomm

Journal Name

RSCPublishing

ARTICLE

Three anhydrous and a dihydrate form of quifenadine hydrochloride: A structural study of the thermodynamic stability and dehydration mechanism

Cite this: DOI: 10.1039/x0xx00000x

Received 00th January 2012,
Accepted 00th January 2012

DOI: 10.1039/x0xx00000x

www.rsc.org/

Artis Kons,[a] Ligita Rutkovska,[a] Agris Bērziņš,[a] Raitis Bobrovs,[ab] and Andris Actiņš,[a]

Crystal structures of dihydrate (DH) and three anhydrous forms (A, B and C) of quifenadine (1-azabicyclo[2.2.2]oct-8-yl-diphenyl-methanol) hydrochloride are presented, and crystal structure information is used to explain and rationalize the relative stability of polymorphs and observed phase transformations. Dehydration mechanism of the hydrate is provided by interpreting the results obtained in studies of crystal structures, dehydration kinetics and thermal analysis. Structural analysis is used to explain the observed relative stability of the anhydrous phases and the hydrate. The crystal structures have been determined either from single crystal (form DH) or from powder diffraction data (forms A, B and C). All three polymorphs consist of similar hydrogen bonded tetramers, and the structural differences arise due to differences in conformation or/ and molecular packing.

Introduction

Polymorphism is the ability of compounds to crystallize into different crystalline modifications. If solvent molecules are incorporated in the crystal lattice along with the host molecules in either stoichiometric or nonstoichiometric ratio, then the resulting phase is called solvate or pseudopolymorph. Polymorphism and pseudopolymorphism of an active pharmaceutical ingredient (API) have an influence on its solubility, bioavailability and stability. Therefore, identification of polymorphs and pseudopolymorphs, comparison of their physicochemical properties and understanding conditions of transformations between crystalline forms are very important[1–3].

From pharmaceutical and supramolecular point of view, the knowledge of polymorph and pseudopolymorph crystal structures gives general information about their stability, formation pathways and also physicochemical properties. Moreover, studies on the polymorphism of organic systems can lead to generalization of the fundamental aspects of the structure-property relationship.[4,5] Therefore, crystal structure determination of pharmaceutically active compounds during the crystalline phase screening process is advisable.

Commonly, crystal structure is determined from single crystal X−ray diffraction data. However, many crystalline solids cannot be prepared in a form of appropriate single crystal. In such a case, powder X-ray diffraction methods can be used to extract structural information. The development of the direct-space approaches for structure solution have given the opportunity to solve crystal structure even from diffraction data recorded using laboratory X-ray powder diffraction instrumentation.[6,7]

Quifenadine (1-azabicyclo[2.2.2]oct-8-yl-diphenyl-methanol) – a quinuclidine derivative, is antihistaminic agent that decreases the impact of histamine by blocking histamine H1-receptors in the peripheral tissues and activates enzyme diamine oxidase (histaminase).[8,9] To the best of our knowledge there are no reports on the existence of polymorphs or solvates of quifenadine hydrochloride.

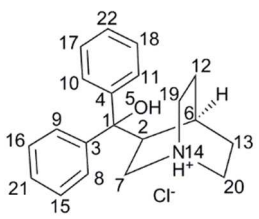

Figure 1. Molecular structure of quifenadine hydrochloride with the numbering of non-hydrogen atoms.

In the present paper, thermal analytical techniques (differential thermal analysis, thermogravimetric analysis and hot-stage

microscopy), powder and single-crystal X-ray diffractometry, and gravimetric moisture sorption studies were employed to characterize the solid state forms of quifenadine hydrochloride. Crystal structures of three anhydrous forms and a hydrate are presented, and crystal structure information is used to explain and rationalize the relative stability of polymorphs and observed phase transformations. Structural transformations during dehydration process of hydrate have been interpreted and the relative stability of anhydrous phases and hydrate have been evaluated.

Experimental section

Materials

Quifenadine hydrochloride (purity >99%) was obtained from JSC Olainfarm (Olaine, Latvia). The sample consisted of commercial racemic mixture of polymorph A. Inorganic compounds and organic solvents of analytical grade were purchased from commercial sources and used without further purification.

Sample preparation

Dihydrate DH was prepared by recrystallizing quifenadine hydrochloride from water and stored at ambient conditions. Single crystals of DH were obtained by slow evaporation from mixture of acetonitrile/ water (95/5 v/v) and stored in mother liquor at ambient conditions. Anhydrous form B was obtained by dehydration of DH at 80 ºC or 0% relative humidity and stored over desiccant. Anhydrous form C was prepared by recrystallizing from *n*-butanol or *iso*−butanol and stored at ambient conditions. Anhydrous form A was used without further purification.

Single Crystal X-ray Diffraction (SCXRD)

The single-crystal X-ray diffraction data for quifenadine hydrochloride DH was collected at 173 K on a Nonius Kappa CCD diffractometer using Mo K_α radiation ($\lambda = 0.71073$ Å) and Oxford Cryostream open-flow nitrogen cryostat for sample temperature control. The structure was solved by direct methods in OLEX2[10] software and refined by full-matrix least-squares on F^2 using SHELXL[11]. All non-hydrogen atoms were refined anisotropically. The most disagreeable reflections with $\Delta(F^2)$ value greater than 5 su were omitted (6 reflections with hkl indices: 0 1 2; 2 -3 2; 1 -3 4; 3 -3 2; -2 -2 8 and -2 -1 6). Mercury 3.3[12] software was used for crystal structure analysis and simulation of powder X-ray diffraction patterns based on crystal structure data. Crystallographic face indexing of quifenadine dihydrate was done at room temperature. Face indexing was performed using Collect software[13].

Powder X-ray Diffraction (PXRD)

For routine measurements of phase composition the PXRD patterns were recorded on a Bruker D8 Advance diffractometer using copper radiation (CuK_α $\lambda = 1.54180$ Å) with Bragg-Brentano geometry and LynxEye (1D) detector. The tube voltage and current were set to 40 kV and 40 mA, respectively. The divergence and antiscattering slits were set at 0.6 mm, and the receiving slit was set at 8 mm. The patterns were recorded from 3° to 30° on the 2θ scale, using a scan speed of 0.2 s/0.02°.

For structure determination PXRD patterns were recorded on a Bruker D8 Discover diffractometer using copper radiation (CuK_α $\lambda = 1.54180$ Å) in transmission mode and LynxEye (1D) detector. The tube was employed with voltage and current settings of 40 kV and 40 mA. The sample was loaded into a special glass Nr. 10 capillary (0.5 mm diameter). Capillary spinner (60 rpm) was used to minimize instrumental and sample packing aberrations. The incident beam path of the diffractometer was equipped with a Göbel mirror, Soller slits, and a 0.6 mm divergence slit, while the diffracted beam path was equipped only with Soller slits. The diffraction patterns were recorded from 3 or 5 to 70° on the 2θ scale at a 0.01° step size using a scan speed of 20 s per step.

Structure Determination from Powder X-ray Diffraction Data

Indexing of powder diffraction patterns of quifenadine hydrochloride A, B and C forms was carried out in programs Dicvol91[14] and X-Cell[15,16] using first 25 reflections ($2\theta < 35°$). All forms were indexed with a triclinic unit cell. The cell and diffraction pattern profile parameters were refined using the Pawley method[17] (R_{wp}=2.29%, R_p=1.40% for A; R_{wp}=1.09%, R_p=0.75% for B and R_{wp}=2.33%, R_p=1.77% for C). The space group for all forms was assigned as $P\bar{1}$ with Z=2.

The trial geometry model was generated by optimizing quifenadine molecule using DFT-D within the DMol^3 module[18] in Materials Studio 7 using the PBE functional[19] and a dispersion correction according to Grimme.[20]

Monte Carlo /Simulating Annealing search algorithm in MS Powder Solve package was used to constantly adjust the conformation, position, and orientation of the trial model in the unit cell in order to maximize the agreement between the calculated and the measured diffraction data. The structural solution obtained from the Powder Solve was refined by Rietveld refinement technique based on the measured powder X−ray diffraction pattern. In the Rietveld refinement, cell parameters, the position and orientation of motion groups, torsion angles, thermal vibration, and preferred orientation parameters (using March-Dollase model[21,22]) were optimized to get an optimum crystal structure. Aromatic rings were treated as rigid groups. The final Rietveld refinement showed a good agreement between the observed and the calculated profiles (Figure 2). Relevant crystal data and refinement details for A, B, C and DH are summarized in Table 1.

Journal Name

RSCPublishing

ARTICLE

Table 1. Crystal structure data for quifenadine hydrochloride forms

Cell parameters	A form	B form	C form	DH form
Chemical formula	$C_{20}H_{24}NOCl$	$C_{20}H_{24}NOCl$	$C_{20}H_{24}NOCl$	$C_{20}H_{24}NOCl{\cdot}2H_2O$
Formula weight	329.86	329.86	329.86	365.88
Sample type	Powder	Powder	Powder	Single crystal
Crystal system	Triclinic	Triclinic	Triclinic	Triclinic
Space group	$P\bar{1}$	$P\bar{1}$	$P\bar{1}$	$P\bar{1}$
Temperature	293(2)	293(2)	293(2)	173(2)
a, Å	6.372(2)	6.408(5)	6.449(2)	6.339(1)
b, Å	12.699(5)	9.281(6)	12.951(3)	8.601(2)
c, Å	10.759(4)	18.356(2)	11.222(2)	18.404(5)
α,°	96.03(2)	113.09(3)	97.60(1)	100.02(2)
β,°	98.88(2)	83.62(3)	106.61(2)	92.32(3)
γ,°	80.68(2)	116.50(3)	75.25(2)	103.45(2)
V, $Å^3$	845.9(1)	895.8(1)	862.9(1)	957.5(3)
ρ_{calc}, $g{\cdot}cm^3$	1.295	1.223	1.270	1.269
Z (Z')	2 (1)	2 (1)	2 (1)	2 (1)
R_{wp} (R_p)/R_1 (wR_2), %	2.81 (1.89)	1.41 (0.99)	3.12 (2.32)	4.8 (14.8)

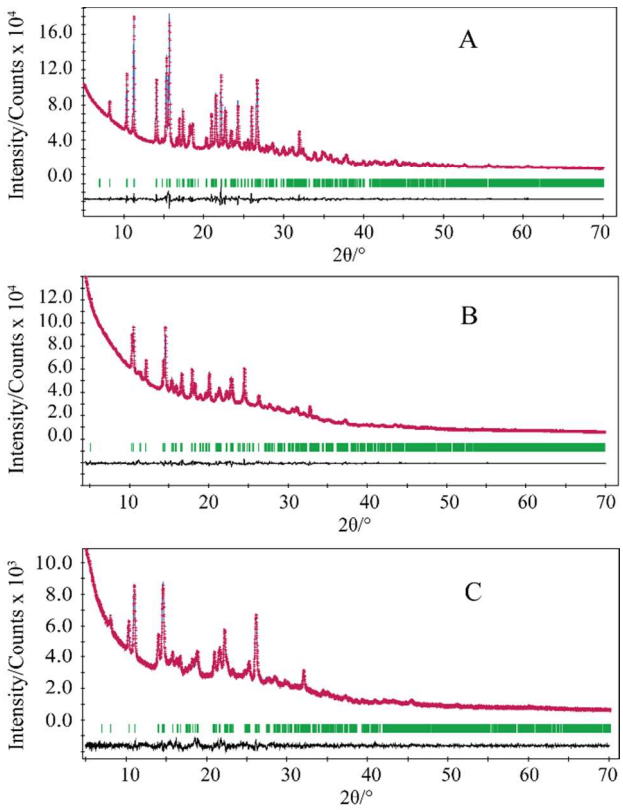

Figure 2. Final Rietveld fit for quifenadine hydrochloride forms A, B and C: red crosses - measured data points; blue line - calculated profile; black line - difference curve; green tick marks - calculated peak positions.

Calculation of lattice and interaction energy in PIXEL

The crystal lattice and interaction energy calculations were performed according to the semiempirical PIXEL methodology (with code provided in the CLP software suite). Empirical parameters were used as provided in the literature.[23] The atom positions for the purposes of this calculation were obtained by standard procedure using RETCIF and RETCOR modules. The hydrogen atom positions were renormalized. Molecular electron density calculations were performed in Gaussian 09[24] at the MP2/6-31G(d,p) level using standard grid parameters. The condensation level 4 and a calculation cutoff value of 40 Å were used.

Differential thermal analysis / thermogravimetric analysis (DTA/TG)

DTA/TG analysis were performed with an Exstar6000 TG/DTA6300 (SII) instrument. Open aluminium pans were used. Heating of samples from 30 °C to 320 °C was performed at the heating rate of 10 °C·min^{-1} under a 100 mL·min^{-1} nitrogen flow. The sample mass was approximately 5−7 mg.

Gravimetric Determination of Water Content

The water sorption and desorption processes of B and DH were measured in desiccators with controlled relative humidity (RH). To provide a variety of RH values saturated salt solutions and P_2O_5 were used. The salts used for this experiment and the corresponding RH values were LiBr (6%), LiCl (11%), CH_3CO_2K (23%), $MgCl_2$ (32%), NaBr (56%), KI (68%), NaCl (75%), KCl (84%), K_2SO_4 (97%), and also P_2O_5 (~0%)[25].

Dehydration kinetics

Nonisothermal experiments were performed at heating rates of 0.5, 2, 3, 4, 5 and 10 °C min^{-1} and isothermal studies were carried out at 30−70 °C using an Exstar6000 TG/DTA6300 (SII) apparatus. For isothermal studies the heater unit was preset to the required temperature allowing fast stabilization of the necessary temperature at the start of the experiment. The sample mass was 6.0 ± 0.5 mg, and the nitrogen flow rate was 100 ± 10 mL min^{-1}.

Hot stage microscopy (HSM)

For thermo-microscopic investigations, a Laborlux 12 PolS (Leitz) polarized light microscope equipped with a heating stage and a Newtronic heating control module was used. The heating rate was 5 ° min^{-1}. Images were collected with Leica Application Suite software from a DFC450 (Leica) digital microscope camera.

Results and discussion

An initial polymorph screening of quifenadine hydrochloride was performed by recrystallization from 16 solvents (water, methanol, ethanol, *n*-propanol, *iso*-propanol, *n*-butanol, *iso*-butanol, acetone, ethyl acetate, acetonitrile, dichloromethane, chloroform, toluene, 1,4-dioxane, dimethylformamide and dimethyl sulfoxide) at variable temperatures. Through the screening process, quifenadine hydrochloride was found to crystallize in three crystalline modifications: two polymorphs (A, C) and dihydrate (DH). Additional polymorph B was obtained by dehydration of DH.

Thermal Analysis

The DTA and TG thermal profiles of all crystalline forms are illustrated in Figure 3. No thermal event was observed for forms A and C in the temperature range prior to the degradation near 320 °C, confirming that these forms are unsolvated. One small exothermal event (at 168 °C) was observed for form B in the temperature range until onset of the degradation. This exothermal effect is attributed to a solid-state phase transition from form B to A as confirmed by PXRD analysis, which substantiates the monotropic relationship between these polymorphs on the basis of the heat of transition rule.[26]

Dehydration of the form DH was observed as an endothermic peak in the DTA over a temperature range from 40 °C to 80 °C and associated weight loss of 9.5% in the TGA. Mass loss of 9.5% corresponds to 1.92 mols of water, which is only slightly below the theoretical value of 2 mols of water per mole of quifenadine hydrochloride. No further weight loss was observed until the material began to degrade at 320 °C. Dehydration product was polymorph B, as confirmed by the PXRD analysis. After the dehydration an exothermic effect observed at 171 °C corresponds to phase transition from polymorph B to form A.

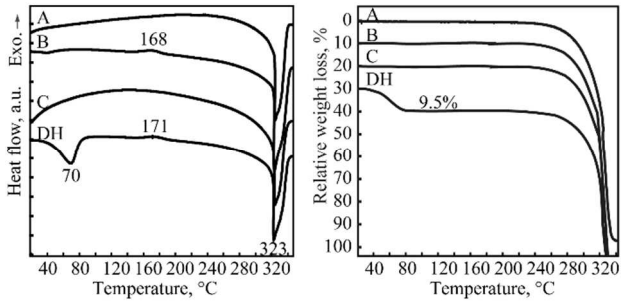

Figure 3. Stacked plots of the DTA and TG curves of quifenadine hydrochloride forms A, B, C and DH.

Thermodynamic Stability of Quifenadine Hydrochloride Polymorphs

To better understand the relative thermodynamic relationships of quifenadine hydrochloride polymorphs, solvent-mediated slurry-bridging (SMSB) experiments were carried out at various temperatures. Mixtures of forms A/B, A/C and B/C were slurried in acetone and tetrahydrofuran at 5 and 25 °C, in acetonitrile at 60 °C and in butyl acetate at 120 °C. That resulted in conversion of mixtures of A/B and A/C to pure form A at all temperatures and similarly mixture of polymorphs B/C converted to form C. These observation indicate that form A is the most thermodynamically stable form at all studied temperatures and form C is more thermodynamically stable than form B.

On the basis of the density rule[26], the most stable crystal structure should have the highest density. As shown in Table 1, the density values calculated from crystal structure data for forms A, B, and C indicate that the stability follows the order of A > C > B. Additionally, comparison of stability of forms A, B and C was performed using calculation of the crystal lattice energy for these forms with PIXEL software. As expected, the form A has the most negative total lattice energy of −382.7 kJ mol^{-1} and therefore is the most stable form at 0 K, followed by form C (−371.4 kJ mol^{-1}) and form B with the highest lattice energy of −361.5 kJ mol^{-1}. Therefore the lattice energy calculations correlate with conclusions obtained from SMSB experiments and crystal density results.

These observations indicate that form A is the most thermodynamically stable form at all temperatures and has monotropic relationship with both forms B and C. Polymorphs B and C also have a monotropic relationship with form C being thermodynamically more stable than form B.

Moisture Sorption Experiments

In moisture sorption/desorption experiments both the weight change and the phase composition of the samples was determined. The moisture sorption/desorption isotherms of quifenadine hydrochloride forms B/DH (Figure 4) shows that the anhydrous form B is stable (i.e., does not absorb water) up to 11% relative humidity (RH). At higher moisture conditions, the sample takes up water, and transforms to DH. The measured mass increase of 9.5% is in agreement with thermogravimetric

measurement (1.92 mol water). By decreasing the humidity, when the RH is less than 6%, the dehydration of from DH occurs and polymorph B is obtained. The distinct steps and presence of hysteresis between the sorption and desorption isotherms are characteristic for stoichiometric hydrates. However, small hysteresis (~5% of RH) shows that this reversible phase transformation has low energy barrier suggesting that crystal structures of these two forms can be similar. The sorption/ desorption isotherms show that DH is very stable hydrate, which releases water only at very low relative humidity, whereas the form B is an unstable anhydrous phase, absorbing water already at 11% RH.

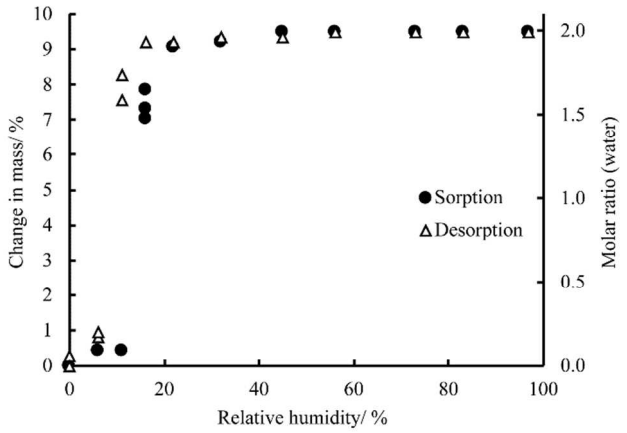

Figure 4. Moisture sorption and desorption isotherms of quifenadine hydrochloride forms B/DH at 30 °C.

Moisture sorption analysis of form C showed that it was stable up to 89% RM (for 2 months), while at higher RM it transformed to form DH, but form A was stable up to 100% RM and transformation to DH was not observed after 2 months.

Analysis of the crystal structures

Structures of polymorphs A, B, and C were determined using powder X-ray diffraction data but structure of DH using single crystal X-ray diffraction data. Crystallographic data of all forms are shown in Table 1. All these crystalline modifications crystallize in *P*$\bar{1}$ space group. Crystal structure of each polymorph contains one quifenadine cation and one chloride anion in the asymmetric unit, whereas dihydrate contains additional two water molecules in the asymmetric unit.

Overlay of powder X-ray diffraction (PXRD) patterns of quifenadine hydrochloride polymorphs and dihydrate are depicted in Figure 5. Each form has a unique and distinguishable PXRD pattern. Comparison of PXRD patterns shows that form A and C has similar positions and intensities of first four peaks suggesting structural similarities. Agreement between the experimental and from crystal structure simulated PXRD patterns of DH confirms the identity of the polycrystalline phase.

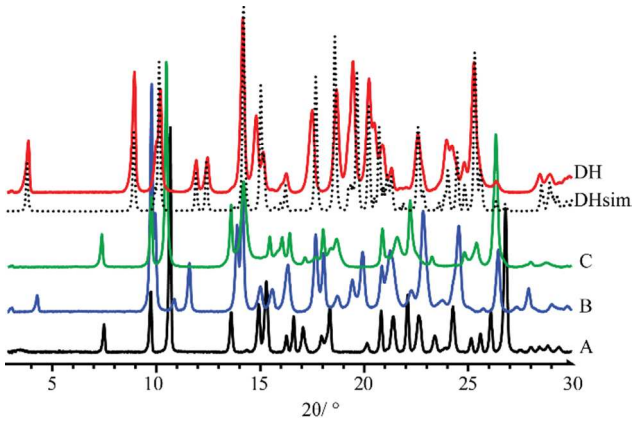

Figure 5. PXRD patterns of quifenadine hydrochloride forms A, B, C and DH.

Quifenadine molecule consists of two terminal phenyl groups, one quinuclidine moiety and one hydroxyl group linked together by a quaternary carbon. The conformational states of the quifenadine cation in all four structures is compared in Figure 6 and the torsion angle values are summarized in Table 2 (numbering of atoms is given in Figure 1). This analysis was carried out using the molecules of identical enantiomers in a quifenadine hydrochloride racemic mixture. It can be seen that the molecular conformation in all four forms is very similar and only minor conformational differences arise mainly due to rotation of phenyl groups and quinuclidine moiety around C(3)−C(1), C(4)−C(1) and C(2)−C(1) bonds. The torsion angle ∠C2−C1−C3−C8 in DH structure is closest to the corresponding angle found in the cation of form B, whereas the torsion angles ∠C2−C1−C4−C10 and ∠C3−C1−C2−C6 in DH structure are closest to the corresponding angles found in the cation of form C.

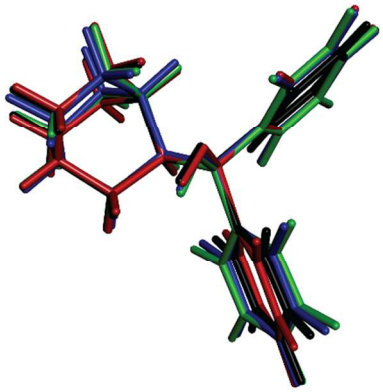

Figure 6. Overlay of the quifenadine cations extracted from the crystal structures of A (black), B (blue), C (red) and DH (green) with superimposed quifenadine moieties.

Table 2. Torsion angle values describing conformational states of quifenadine cations in the crystalline forms A, B, C and DH

	∠C2-C1-C3-C8	∠C2-C1-C4-C10	∠C3-C1-C2-C6
A	-36.9(3)	46.2(3)	174.0(2)
B	−24.0(6)	60.5(10)	179.3(4)
C	−44.1(4)	59.0(4)	172.2(2)
DH	−15.9(2)	61.9(2)	169.88(14)

In quifenadine hydrochloride, the only easily acessible strong hydrogen bond acceptor is the Cl^- anion, and the possible donors allowing the formation of strong hydrogen bonds are the NH^+ group and hydroxyl group. As shown in Figure 7, all three polymorphs have the same hydrogen bonding pattern where two chloride anions interact with two quifenadine cations through N14–H···Cl24 and O5–H···Cl24 bonds and forms a tetramer with graph set $R_4^2(16)$. Slight differences were observed in hydrogen bond geometry and interaction energy between hydrogen bond donor and acceptor moieties in each of these three forms (see Table 3). Form A has the most negative interaction energy between cation and anion moieties, but interaction energy in forms B and C is almost equal. Hydrogen bonding pattern in quifenadine hydrochloride dihydrate structure is more complex due to the presence of two water molecules increasing the number of possible hydrogen bond acceptor and donor sites. In this structure hydrogen bonds are formed between NH^+ group and water molecules. The Cl^- is involved in H-bonding with the three water molecules and also with the -OH group attached to C1. H-bonds between water molecules are also observed. Two quifenadine cations, two chloride anions and two water molecules form a hexamer with te graph set $R_6^4(20)$ through N14–H···O25, O5–H···Cl24 and O25–H···Cl24 bonds(see Figure 7). Two other water molecules form a hydrogen bonded ring with chloride anions with the graph set $R_4^2(8)$. All of the water molecules are also involved in formation of hydrogen bonded chain including chloride anion ($C_3^2(6)$) perpendicular to the H-bonded hexamer $R_4^2(8)$ ring. Therefore the dehydration induces breakage of the hydrogen bond network and six hydrogen bonds are replaced with two new ones. Obviously, the water molecules play a stabilizing role in the quifenadine hydrochloride dihydrate structure by forming efficient hydrogen bonding network, which explains its stability.

Table 3. Geometry and energy data of hydrogen bonds in quifenadine hydrochloride forms A, B, C and DH

Interaction	D···A, Å	D-H···A, °	Interaction energy, kJ mol^{-1}
Form A			
O5–H···Cl24	3.096(4)	156	-423.5
N14–H···Cl24	3.010(4)	153	-446.6
Form B			
O5–H···Cl24	3.152(5)	159	-413.9
N14–H···Cl24	3.042(5)	150	-442.2
Form C			
O5–H···Cl24	3.177(7)	151	-411.5
N14–H···Cl24	3.034(7)	151	-444.6
Form DH			
O5–H···Cl24	3.197(2)	165	–[a]
N14–H···O26	2.727(2)	166	–
O25–H48···Cl24	3.171(2)	172	–
O25–H49···Cl24	3.177(2)	179	–
O25–H··· O26	2.732(2)	165	–
O26–H···Cl24	3.179(2)	171	–

[a] It was not possible to perform interaction energy calculation using PIXEL code because of four chemical entities in the asymmetric unit

As shown in Figure 8, the forms A and C have the same monolayered molecular packing pattern where all neighboring molecules are in antiparallel orientation. The 2D pattern is defined by the same type of layers. However, there are marked differences between the packing of the forms A and C, and the form B. The molecular packing of the form B has bilayered pattern where neighboring molecules are in the same direction and molecules in each layer are in opposite orientation to those in an adjacent layer. The molecular packing of the form B has more distinguishable hydrophobic and hydrophilic layers than in forms A and C where tetramers are packed more efficiently.

The molecular packing of the form DH share common features with that of the form B. The 2D structural pattern of DH is defined by the same molecular orientation and the same arrangement of the layers with respect to each other. The only difference is the inclusion of water molecules, which are located in structural channels between hydrophilic quinuclidine groups and chloride anions. Therefore DH is a channel hydrate. Besides, water molecules are involved in the main hydrogen bonding network, which makes this hydrate stoichiometric. Due to the high structural packing similarity it is clear why the dehydration of DH leads to the form B instead of the A or C. This transition does not change the parallel orientation of quifenadine cations in the crystal structure, it only decreases the distance between the quifenadine moieties. Transformation of DH to A or C requires a significant amount of molecular reorganization and therefore this transition is unfavourable, as is the reverse process, explaining the observations in moisture sorption experiments.

To compare the packing efficiency and therefore the stability in all four forms, calculation of the packing index for these forms has been performed with the PLATON[27] software. PLATON calculations yielded a 73.1, 71.7, 69.1 and 68.4% packing indices for forms A, C, B and DH respectively, which is in agreement with thermodynamic stability results for these polymorphic forms. The lowest packing index of form DH,

however, suggests that presence of water molecule channels does not lead to very efficient packing, but the stability of this crystal structure is provided by energetically efficient hydrogen bonding network provided by the insertion of water molecules.

In order to better explore the differences between very similar forms A and C, full geometry optimization of these two crystal structures were performed using the DFT-D method within Quantum Espresso.[28] Obtained results indicated that between forms A and C there are only small energy barrier because after geometry optimization of both experimental structures almost identical structure was obtained. Therefore the only explanation why form C was obtained from n-butanol or *iso*–butanol instead of very similar form A can be based on the presence and strength of some specific interactions between the solvent molecules and quifenadine and chloride moieties during the crystallization, resulting in slightly different molecular packing, which interestingly was not able to regroup to very similar but thermodynamically more stable structure A.

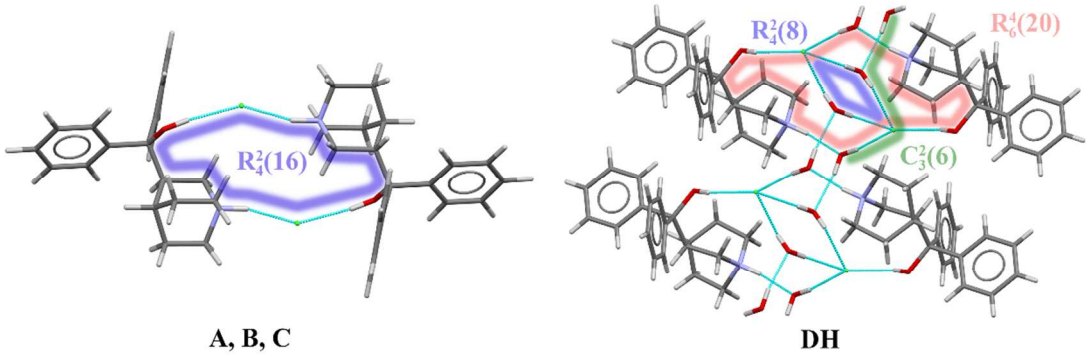

Figure 7. The hydrogen bonding patterns in quifenadine hydrochloride forms A, B, C and DH.

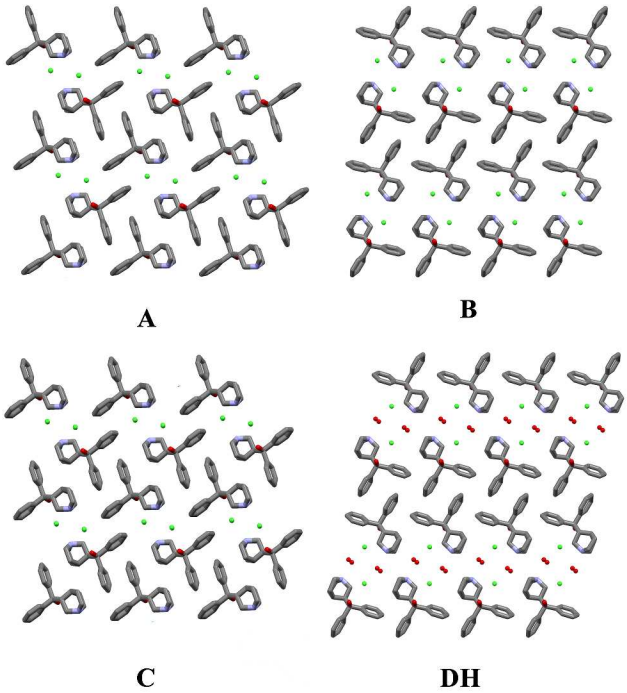

Figure 8. The molecular packing in quifenadine hydrochloride forms A, B, C and DH (hydrogen atoms have been omitted for clarity).

Dehydration kinetics

Dehydration kinetic model and activation energy (E_a) was determined in isothermal and non-isothermal mode to better understand the dehydration mechanism of DH. It is recommended to analyze the solid-state kinetics over selected fraction dehydrated (α) values because errors are usually higher at very low and high fraction dehydrated values,[29] therefore, determination of activation energy and model fitting was performed for the data $0.2 \leq \alpha \leq 0.8$. The isothermal and nonisothermal dehydration kinetics of DH were first analyzed by Friedman's isoconversional method. Figure 9 gives calculated E_a values as a function of fraction dehydrated α for dehydration of DH in isothermal (left) and non-isothermal (right) mode. The activation energy was determined to be 59±4 kJ mol^{-1} and 62±5 kJ·mol^{-1} in isothermal and non-isothermal mode respectively. The matching values of E_a calculated for both isothermal and nonisothermal mode suggest that the dehydration mechanism in both modes is the same. To identify an acceptable kinetic model, linear regression correlation coefficient (R^2) for the plot of the $g(\alpha)$ versus t was calculated for the most common solid state kinetic models. Equally high correlation coefficients were found for both the one-dimensional phase boundary reaction model R1 (R^2=0.9995) and two-dimensional phase boundary reaction model R2 (R^2=0.9994). Then the reconstruction of the dehydration curves was performed to identify the most appropriate reaction model between R1 and R2. Figure 10 gives experimental and theoretical dehydration isotherms (fraction dehydrated versus time) obtained from TGA in isothermal mode at different temperatures. As shown in Figure 10, model R1 provides a good description of the isothermal dehydration kinetics over $0.2 \leq \alpha \leq 0.8$ range of the fraction dehydrated. Besides, R1 is a rational dehydration model for channel type hydrate with structurally close dehydration product, as the dehydration process most likely occurs by the movement of phase boundary in the direction of the water channels. At $\alpha>0.8$, experimental isothermal α-time plots deviated from the linear relationship (and therefore from kinetic model R1) because the dehydration

process became slower. Although similar deviation is characteristic to kinetic model R2, in this case R2 provides worse fit to the experimental data, see Figure 10. Therefore the observed deviation indicated that at the end of the dehydration the mechanism was changing, which probably could be caused by the presence of particles with different sizes, as large particles dehydrate slower than smaller particles.

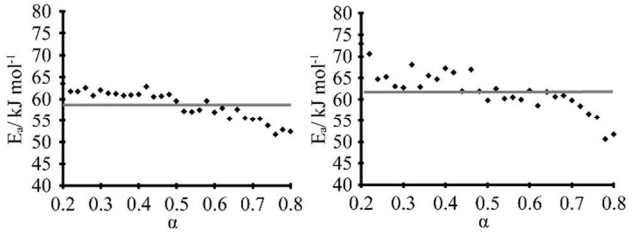

Figure 9. Dehydration E_a values as a function of fraction dehydrated α in isothermal (left) and non-isothermal (right) mode.

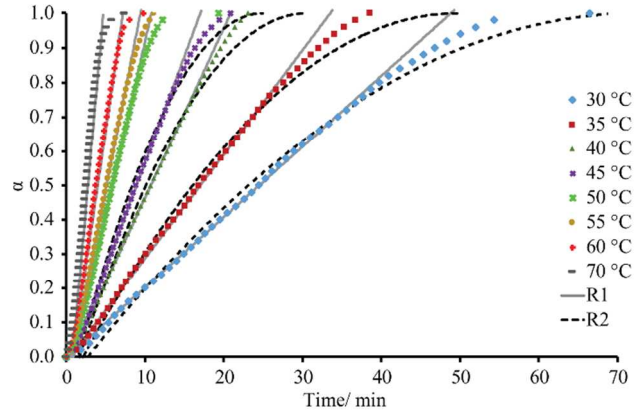

Figure 10. Experimental and theoretical representation of the dependence of fraction dehydrated (α) on time obtained from TGA at different temperatures in isothermal mode.

Hot Stage Microscopy

The direct microscopic observations can provide useful information to identify and substantiate the best fitting kinetic model obtained from mathematical analysis of the kinetic data. As many solid-state kinetics models are based on geometric model functions, adequacy of these models can be verified by visual observation of the dehydration reaction.[30,31]

Photomicrographs taken during the dehydration of DH using hot stage microscopy are shown in Figure 11 and crystal morphology determined by single crystal face indexing is shown in Figure 12. From Figure 12 it can be seen that there are channels containing water molecules along the *a*-axis in the DH structure and during the dehydration water escapes through these channels. This result fits with the observations from hot stage microscopy in Figure 11, where the dehydration process initiates from both ends of the crystal and by increasing the temperature the reaction boundary slowly moves inwards to the center of the crystal. Therefore the microscopic observations confirm the R1 reaction model, where dehydration process is in one-dimension, and water molecules escape through the water channels along the *a*-axis.

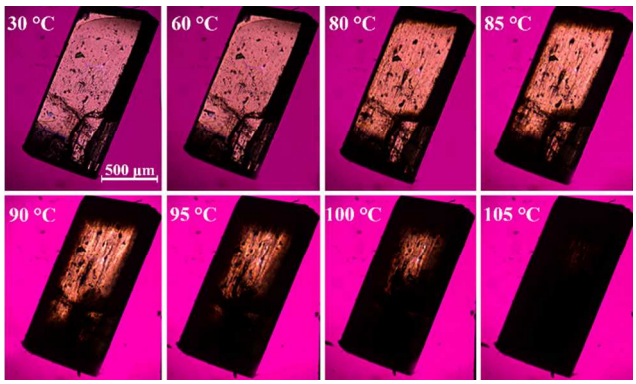

Figure 11. Photomicrographs of the dehydration process of DH form.

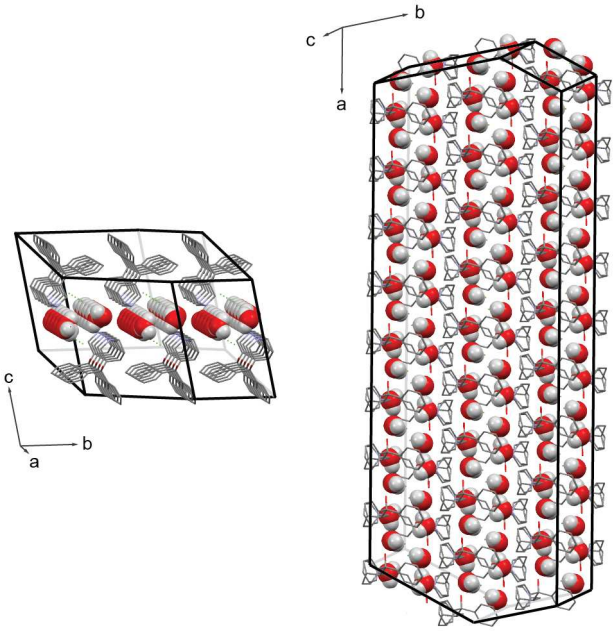

Figure 12. Determined crystal morphology of DH crystal showing water channels along *a*- axis.

Conclusions

Crystallization of quifenadine hydrochloride from 16 different solvents produced two anhydrous forms (A,C) and a dihydrate (DH), while the dehydration of DH produced another new polymorph (B). The same hydrogen bonding pattern (hydrogen bonded tetramer consisting of two quifenadine cations and two chloride anions) was observed in the crystal structures of all three polymorphs. Thermodynamic stability of the polymorphs was established by SMSB experiments and calculation of the crystal lattice energy. These results demonstrated that form A is the most thermodynamically stable form, followed by form C and then form B, besides, all three polymorphs have monotropic relationship to each other.

In DH hydrogen bonds form complex network, with water molecules playing a stabilizing role. Water molecules are located in structure channels and dehydration produces structurally similar polymroph B. Therefore the solid-state hydration/ dehydration transformation DH ↔ B is reversible at ambient conditions and depends on the relative humidity.
The dehydration of form DH was studied using various experimental methods. It was determined that the dehydration proceeds by the one-dimensional phase boundary reaction model (R1) in which the water molecules escape through the structure channels along the *a*-axis.

Supporting information

CCDC 1051731, 1051732, 1051733, and 1051734 contains the supplementary crystallographic data for the structures of **DH**, **A**, **B**, **C** respectively. These data can be obtained free of charge via http://www.ccdc.cam.ac.uk/conts/retrieving.html (or from the Cambridge Crystallographic Data Centre, 12, Union Road, Cambridge CB2 1EZ, UK; fax: +44 1223 336033).

Acknowledgements

We wish to thank the Riga Technical University Institute of Polymer Materials for the provided opportunity to carry out hot-stage microscopy measurements, Inese Sarceviča for the help with single crystal structure determination and Formulation and Drug Delivery Research Group, School of Pharmacy and Biomolecular Sciences, Liverpool John Moores University for the possibility to carry out calculations with Material Studio.

Notes and references

[a] Faculty of Chemistry, University of Latvia, Kr. Valdemara iela 48, Riga, Latvia
[b] Formulation and Drug Delivery Research Group, School of Pharmacy and Biomolecular Sciences, Liverpool John Moores University, Liverpool, UK

† Footnotes should appear here. These might include comments relevant to but not central to the matter under discussion, limited experimental and spectral data, and crystallographic data.
Electronic Supplementary Information (ESI) available: [details of any supplementary information available should be included here]. See DOI: 10.1039/b000000x/

1 S. Ito, M. Nishimura, Y. Kobayashi and S. Itai, *Int. J. Pharm.*, 1997, **151**, 133–142.

2 H. G. Brittain, *J. Pharm. Sci.*, 2012, 101, 464–484.

3 R. Hilfiker, ed. W. Beckmann, Wiley-VCH Verlag GmbH & Co. KGaA, Weinheim, Germany, 2013.

4 J. Bernstein, *Cryst. Growth Des.*, 2011, **11**, 632–650.

5 G. P. Stahly, *Cryst. Growth Des.*, 2007, 7, 1007–1026.

6 W. I. F. David, K. Shankland, J. Van De Streek, E. Pidcock, W. D. S. Motherwell and J. C. Cole, *J. Appl. Crystallogr.*, 2006, **39**, 910–915.

7 W. I. F. David and K. Shankland, *Acta Crystallogr. A.*, 2008, **64**, 52–64.

8 United States Patent, US4117139 A, 1978.

9 L. Makarov, L. Balykova, O. Soldatova, V. Komolyatova and V. Serebruany, *Am. J. Ther.*, 2012, **17**, 396–401.

10 O. V. Dolomanov, L. J. Bourhis, R. J. Gildea, J. a. K. Howard and H. Puschmann, *J. Appl. Crystallogr.*, 2009, **42**, 339–341.

11 G. M. Sheldrick, *Acta Crystallogr. A.*, 2008, **64**, 112–22.

12 C. F. Macrae, I. J. Bruno, J. A. Chisholm, P. R. Edgington, P. McCabe, E. Pidcock, L. Rodriguez-Monge, R. Taylor, J. van de Streek and P. A. Wood, *J. Appl. Crystallogr.*, 2008, **41**, 466–470.

13 Nonius BV, Nonius KappaCCD Collect, 1998.

14 A. Boultif and D. Louër, *J. Appl. Crystallogr.*, 1991, **24**, 987–993.

15 A. Boultif and D. Louër, *J. Appl. Crystallogr.*, 2004, **37**, 724–731.

16 M. A. Neumann, *J. Appl. Crystallogr.*, 2003, **36**, 356–365.

17 G. S. Pawley, *J. Appl. Crystallogr.*, 1981, **14**, 357–361.

18 B. Delley, *J. Chem. Phys.*, 1990, **92**, 508–517.

19 J. Perdew, K. Burke and M. Ernzerhof, *Phys. Rev. Lett.*, 1996, **77**, 3865–3868.

20 S. Grimme, *J. Comput. Chem.*, 2006, **27**, 1787–1799.

21 March, *Z. Krist.*, 1932, **81**, 285–297.

22 W. a. Dollase, *J. Appl. Crystallogr.*, 1986, **19**, 267–272.

23 A. Gavezzotti, *New J. Chem.*, 2011, 35, 1360–1368.

24 M. J. Frisch, G. W. Trucks, H. B. Schlegel, G. E. Scuseria, M. A. Robb, J. R. Cheeseman, G. Scalmani, V. Barone, B. Mennucci, G. A. Petersson, H. Nakatsuji, M. Caricato, X. Li, H. P. Hratchian, A. F. Izmaylov, J. Bloino, G. Zheng, J. L. Sonnenberg, M. Hada, M. Ehara, K. Toyota, R. Fukuda, J. Hasegawa, M. Ishida, T. Nakajima, Y. Honda, O. Kitao, H. Nakai, T. Vreven, J. A. J. Montgomery, J. E. Peralta, F. Ogliaro, M. Bearpark, J. J. Heyd, E. Brothers, K. N. Kudin, V. N. Staroverov, R. Kobayashi, J. Normand, K. Raghavachari, A. Rendell, J. C. Burant, S. S. Iyengar, J. Tomasi, M. Cossi, N. Rega, J. M. Millam, M. Klene, J. E. Knox, J. B. Cross, V. Bakken, C. Adamo, J. Jaramillo, R. Gomperts, R. E. Stratmann, O. Yazyev, A. J. Austin, R. Cammi, C. Pomelli, J. W. Ochterski, R. L. Martin, K. Morokuma, V. G. Zakrzewski, G. A. Voth, P. Salvador, J. J. Dannenberg, S. Dapprich, A. D. Daniels, O. Farkas, J. B. Foresman, J. V Ortiz, J. Cioslowski, D. J. Fox, J. Montgomery, J. A., J. E. Peralta, F. Ogliaro, M. Bearpark, J. J. Heyd, E. Brothers, K. N. Kudin, V. N. Staroverov, R. Kobayashi, J.

Normand, K. Raghavachari, A. Rendell, J. C. Burant, S. S. Iyengar, J. Tomasi, M. Cossi, N. Rega, N. J. Millam, M. Klene, J. E. Knox, J. B. Cross, V. Bakken, C. Adamo, J. Jaramillo, R. Gomperts, R. E. Stratmann, O. Yazyev, A. J. Austin, R. Cammi, C. Pomelli, J. W. Ochterski, R. L. Martin, K. Morokuma, V. G. Zakrzewski, G. A. Voth, P. Salvador, J. J. Dannenberg, S. Dapprich, A. D. Daniels, Ö. Farkas, J. B. Foresman, J. V Ortiz, J. Cioslowski and D. J. Fox, 2009.

25 L. Greenspan, *J. Res. Natl. Bur. Stand. Sect. A Phys. Chem.*, 1977, **81A**, 89–96.

26 A. Burger and R. Ramberger, *Microchim. Acta*, 1979.

27 A. L. Spek, *Acta Crystallogr. D. Biol. Crystallogr.*, 2009, **65**, 148–155.

28 P. Giannozzi, S. Baroni, N. Bonini, M. Calandra, R. Car, C. Cavazzoni, D. Ceresoli, G. L. Chiarotti, M. Cococcioni, I. Dabo, A. Dal Corso, S. de Gironcoli, S. Fabris, G. Fratesi, R. Gebauer, U. Gerstmann, C. Gougoussis, A. Kokalj, M. Lazzeri, L. Martin-Samos, N. Marzari, F. Mauri, R. Mazzarello, S. Paolini, A. Pasquarello, L. Paulatto, C. Sbraccia, S. Scandolo, G. Sclauzero, A. P. Seitsonen, A. Smogunov, P. Umari and R. M. Wentzcovitch, *J. Phys. Condens. Matter*, 2009, **21**, 395502.

29 A. Khawam and D. R. Flanagan, *Thermochim. Acta*, 2005, **429**, 93–102.

30 V. Koradia, H. L. D. E. Diego, M. R. Elema and J. Rantanen, 2010, **99**, 3966–3976.

31 A. K. Galwey, *Thermochim. Acta*, 2000, **355**, 181–238.

Table of Contents entry

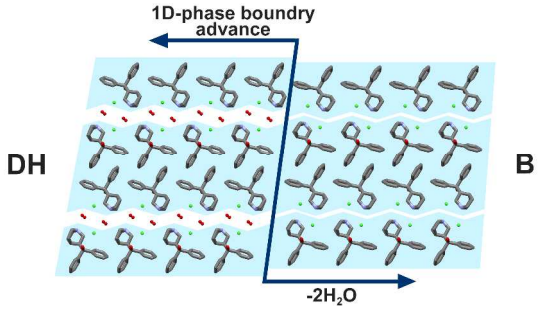

Crystal structures of dihydrate and three anhydrous forms of quifenadine hydrochloride are presented, and crystal structure information is used to explain the relative stability of polymorphs and observed phase transformations.